Imaging viscoelasticity by force modulation with the atomic force microscope

M. Radmacher, R. W. Tillmann, and H. E. Gaub
Physikdepartment Technische Universität München, 8046 Garching, Germany

ABSTRACT Force modulation and phase sensitive detection was used to image soft surfaces with the atomic force microscope. This force modulation microscopy allows the simultaneous recording of images of the surface profile, the storage modulus, and the loss modulus of the sample. A theoretical treatment of the elastic tip–sample interaction is given. As examples, images of Langmuir–Blodgett films of a polymeric amphiphile and of a structured fatty acid are presented.

INTRODUCTION

The atomic force microscope (AFM) (1–3), has become a widely used instrument in a broad range of disciplines. Its unique feature, to image samples at molecular resolution in physiological ambient, makes this instrument ideally suited for applications in life sciences (3–6). Like all near field microscopes, the AFM profiles the topology of the sample by scanning a probe over the sample surface. The AFM does it in such a way that the force between probe and sample stays constant. The resulting image is thus an iso-force relief of the sample. It is intriguing, that the AFM may also be used to probe certain mechanical properties of the sample by measuring the response of the sample to an increased or decreased load by the tip (7). In a so-called force scan, where the probe is positioned on a desired spot on the sample, quantitative information about the elastic constants of the sample may be obtained under certain conditions (8–10). Here we discuss a new technique, where the dynamic response of the sample is measured and additional information about the viscosity is gained. We perform these measurements while scanning the sample, providing a viscoelasticity image of the sample.

MATERIALS AND METHODS

LB-films were prepared with a home-built trough described elsewhere in detail (11). A chloroformic solution of monomeric diamino-diethylene glycol-pentacosadiynoic acid (12) (DPDA) (kind gift from Biocircuits, Burlingame CA) was spread on pure water (Milli Q Systems, Molsheim France). The film was compressed to a final pressure of 30 mN/m and UV polymerized with a Hg-pen ray for 30 s in air. For details of the preparation see (12). The pressure dropped by about 15 mN/m during polymerization. This film was transferred by the use of LB-technology to a cleaned silicon wafer and imaged after 2 days of storage in a dessicator in the AFM. For the experiments with DPDA films containing DMPC (di-palmitoyl-phosphatidyl-choline) the sample was prepared the same way, except that a fraction of 30% of DMPC was added to the chloroformic solution. Arachic acid was applied to the air–water interface from chloroformic solution. As subphase, a buffer solution of 1 mMol HEPES and 0.5 mMol $CdCl_2$ at pH 7 was used. The monolayer was compressed to a surface pressure of 35 mN/m and a trilayer was transferred on a silicon wafer as support by standard LB-techniques. The film was partially ablated by irradiation with UV-light (13). All chemicals were from Sigma, (Deisenhofen, FRG) unless otherwise noted.

Thermally oxidized silicon wafers (⟨100⟩ p-Type with an oxide-layer of 180 nm) (Wacker, Burghausen, FRG) were cleaned with Hellmanex (Hellma, Müllheim, FRG) for 30 min in an ultrasonic bath. After rinsing several times with pure water (Milli-Q-Systems, Molsheim, France) they were ultrasonificated for 30 min in pure water, rinsed again several times with pure water, and ultrasonificated in methanol (HPLC-quality; Aldrich, Milwaukee, Wisconsin). These wafers were used as a calibration substrate (see below) or as support for LB films.

EXPERIMENTAL SETUP

The home-built AFM (see Fig. 1), which was used in this study, is described in detail elsewhere (14). The sample is mounted on an xyz piezo scan tube with a 15 μm scan range. As probes, commercially available silicon nitride cantilevers with integrated tips (Digital Instruments, Santa Barbara, CA) were used. The cantilevers have a force constant of about 64 mN/m. The force constant is known to vary by a factor of 2 within the same batch of this type of tips.[1] The deflection of the cantilever is measured by a position-sensitive two-segment photo diode and fed into the feedback-loop that controls the height z of the sample in a way that the deflection stays constant (15). For force modulation, a sinusoidal signal is added to the z voltage of the piezo. This leads to an additional deflection of the cantilever and thus to a variation of the force between tip and sample. The extent to which this force deforms the sample depends on the viscoelastic properties of the sample (see Fig. 2). The deflection signal is fed into two two-phase lock-in amplifiers (EG&G 5208), which output amplitude and phase shift of the harmonic and the second harmonic signal, respectively. A computer (Macintosh II fx) records the lowpass filtered z-signal and the four lock-in signals. All five signals may be displayed simultaneously while scanning. Images are recorded during back-and-forth scan, which

Address correspondence to Dr. Hermann E. Gaub, Fakultät für Physik, Technische Universität München, Lehrstuhl für Biophysik E-22, D-8046 Garching, Germany.

[1] Regarding the integrated tips, see Hoh, J. H., J. P. Cleveland, C. B. Prater, J. P. Revel, and P. K. Hansma. 1992. Quantized adhesion detected with the atomic force microsope. *J. Am. Chem. Soc.* 114:4917–4918.

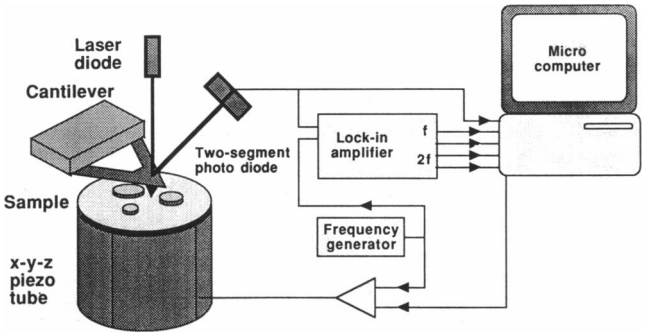

FIGURE 1 Schematics of an atomic force microscope with optical lever detection. Also outlined are the electronics extensions for imaging viscoelastic properties.

provides additional information on the sample-like distortions (16) and differences in the local friction (3).

Phase shift and amplitude of the response of the cantilever are both a function of the mechanical and also of the electronical setup. Due to mechanical resonances, the amplitude and the phase of the instrument are extremely frequency-dependent. For a quantitative analysis of the data it is therefore necessary to normalize the measured response with the apparatus transfer function. The latter was separately measured on the bare substrate, which is incompressible compared to our samples. In our case this was a silicon wafer, which was cleaned with greatest care (17). The apparatus transfer function was measured for different cantilevers, different wafers, and different media between tip and sample, and appeared to be independent of these parameters.

THEORY OF THE FORCE MODULATION MICROSCOPY

The contact between two smooth elastic surfaces was first investigated by Hertz, who proposed a simple model, where both the size and shape of contact followed from the elastic properties of the bodies. For two spheres of radius R_1 and R_2 pressed together under a load F_0 the radius a_0 of the circle of contact is given by:

$$a_0^3 = \frac{3}{4}\pi(k_1 + k_2)\frac{R_1 R_2}{R_1 + R_2} F_0 \qquad (1)$$

k_1 and k_2 are the elastic constants of the material of each sphere that are given by:

$$k_1 = \frac{1 - \nu_1}{\pi E_1} \quad k_2 = \frac{1 - \nu_2}{\pi E_2} \qquad (2)$$

where E and ν are the Young modulus and the Poisson ratio, respectively. From Eq. 1, it follows that the centers of the spheres approach each other by a distance d, given by:

$$d^3 = \frac{9}{16}\pi^2(k_1 + k_2)^2\frac{R_1 + R_2}{R_1 R_2} F_0^2. \qquad (3)$$

This relation holds only for isotropic bodies. Also, if adhesion or wetting of the two surfaces is taken into account, this relation has to be modified accordingly (see Fig. 3) (18). The influence of such effects on our measurements will be discussed further below. Because in our experiments the sample is much softer than the tip, we can assume the tip to have a negligible elastic constant. This, and the fact that the sample is planar, reduces Eq. 3 to the following expression, where R is the radius of the tip:

$$d^3 = \frac{9}{16}\frac{\pi^2 k^2}{R} F_0^2. \qquad (4)$$

Because only the sample is deforming, d is equivalent to the indentation of the sample (see Fig. 3 *a*). In force modulation microscopy the load F is varied around an equilibrium load F_0. Therefore we expand formula 4 and obtain as a first-order approximation the linearized form (see Fig. 4):

$$\frac{\partial F_n}{\partial d} = K_{eff} = \left(\frac{6}{\pi^2}\frac{1}{k^2} F_0 R\right)^{1/3} \qquad (5)$$

The expansion of formula 4 to the second order leads to the anharmonic distortion:

$$\frac{\partial^2 F_n}{\partial d^2} = \beta = \left(\frac{4R^2}{3\pi^4 k^4}\right)^{1/3} \cdot F_0^{-1/3}. \qquad (6)$$

Thus it appears that within the limitations of the Hertz model, the linear term will dominate the high force re-

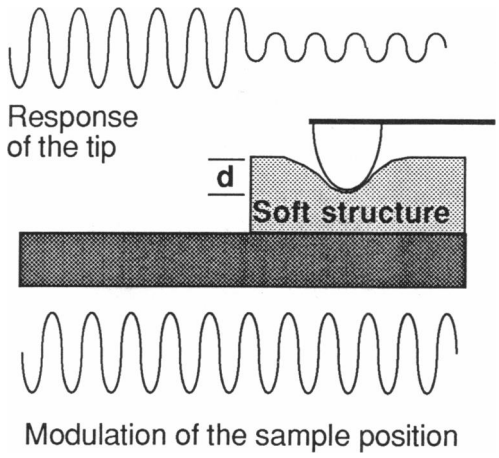

FIGURE 2 Schematics of the viscoelastic measurement with the AFM. The modulation of the vertical sample position leads to a modulation of the force between tip and sample. This force modulation results in an indentation of the sample depending on its elastic properties. The amplitude and the phase shift between excitation and response may be analyzed in terms of the viscoelastic theory.

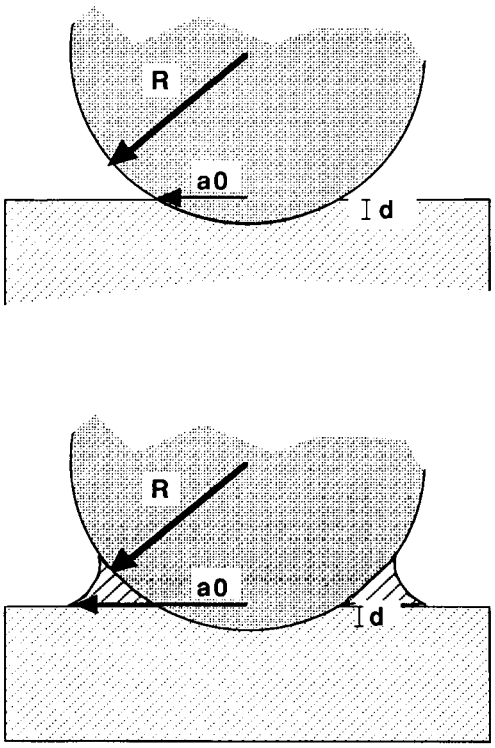

FIGURE 3 The Hertzian model describes the deformation of two elastic bodies. (Top) A virtually incompressible sphere of radius R is pressed by a force F on an elastic sample, which reacts by an indentation d. The radius of contact between sphere and sample is labeled a_0. (Bottom) Additional adhesive forces like van der Waals attraction or wetting of the sphere by the sample or wetting by a water film of the ambient lead to a larger contact area a_0 and to an additional load.

gime. Whether or not the anharmonic term will contribute significantly at low forces will be calculated in the following based on typical experimental values and for Langmuir–Blodgett films as samples. The sample will still be assumed to be isotropic.

Typical values are: 9 GPa for the Young's module of LB-films (19), 10 nm for the radius of an AFM-tip (3) and 10 nN for the applied load. With the parameters given above k_{eff} and β will have the values:

$$k_{eff} = 17 \text{ N/m} \quad \beta = -0.003 \text{ N/m}^2.$$

The elastic force F_H, given by the Hertz model will be in the approximated form:

$$F_H = F_0 + k_{eff} \cdot \delta + \tfrac{1}{2} \cdot \beta \cdot \delta^2. \tag{7}$$

This force will be balanced by the force exerted from the cantilever to the sample $k_c \cdot l$, where k_c is the force-constant of the cantilever and l is its deflection from the zero point. The sample-height z is additionally modulated around its equilibrium position by the external modulation:

$$z = l_0 + z_0 \cdot \sin(\omega t) \tag{8}$$

The sample modulation will lead to a deflection of the cantilever diminished by the sample indentation δ. This leads to a force F_c exerted by the cantilever:

$$F_c = k_c(l_0 + z_0 \cdot \sin(\omega t) - \delta). \tag{9}$$

These two forces have to be in balance:

$$F_0 + k_{eff} \cdot \delta + \tfrac{1}{2} \cdot \beta \cdot \delta^2 = k_c(l_0 + z_0 \cdot \sin(\omega t) - \delta). \tag{10}$$

Thus the equilibrium load on the sample is given by:

$$F_0 = k_c \cdot l_0. \tag{11}$$

This simplifies Eq. 10 to:

$$k_{eff} \cdot \delta + \tfrac{1}{2} \cdot \beta \cdot \delta^2 = k_c(z_0 \cdot \sin(\omega t) - \delta). \tag{12}$$

After some algebraic rearrangement of Eq. 12 we find:

$$\delta = \frac{k_{eff} + k_c}{\beta} \cdot \left[-1 \pm \sqrt{1 + \frac{k_c \cdot z_0 \cdot \beta}{(k_{eff} + k_c)^2} \cdot \sin(\omega t)} \right]. \tag{13}$$

Only the positive solution of the quadratic equation is physically meaningful, because the indentation δ has to be a positive number. Eq. 13 can be approximated by expansion of the square root to second order:

$$\delta = \frac{k_{eff} + k_c}{\beta} \cdot \left[\frac{1}{2} \cdot \frac{k_c \cdot z_0 \cdot \beta}{(k_{eff} + k)^2} \cdot \sin(\omega t) - \frac{1}{8} \cdot \left(\frac{k_c \cdot z_0 \cdot \beta}{(k_{eff} + k_c)^2} \cdot \sin(\omega t) \right)^2 \right]. \tag{14}$$

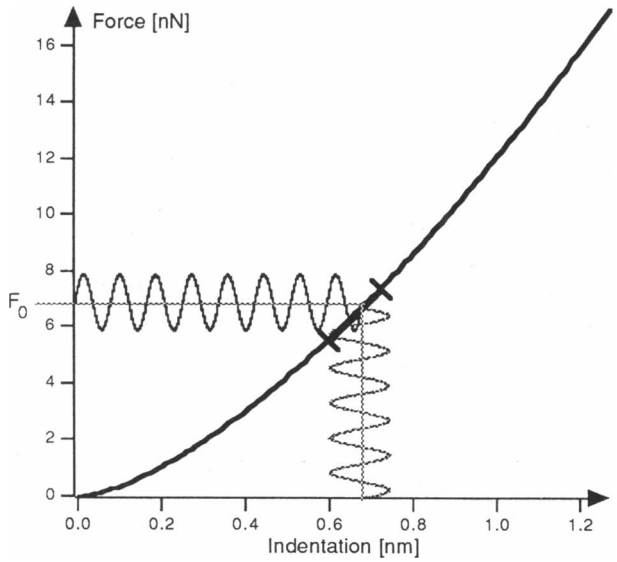

FIGURE 4 Hertzian potential for the samples used in this study. Values for the simulation are: 9 GPa for the Young module and 10 nm for tip radius. The linearization is depicted for an typical load and the principle of force modulation, which leads to an indentation variation as well.

We can extract the harmonic and the anharmonic part of the indentation:

$$\delta_1 = \frac{k}{k_{eff} + k_c} \cdot z_0 \cdot \sin(\omega t) \tag{15}$$

$$\delta_2 = -\frac{1}{16} \frac{\beta \cdot k^2}{(k_{eff} + k_c)^2} \cdot z_0^2 \cdot \cos(2\omega t). \tag{16}$$

With a typical value for the modulation of the piezo height of 10 nm, this results in an amplitude of the harmonic response of 0.4 Å and of an amplitude for the anharmonic response of 10^{-15} Å. This calculation demonstrates that for our experimental conditions anharmonic effects due to the Hertz model are negligible. Wetting or adhesion will only shift the zero force but will otherwise not significantly change the modulation amplitude. These calculations also show that for soft samples like LB films, standard integrated cantilever are stiff enough to give rise to a well detectable harmonic response.

LINEAR VISCOELASTIC THEORY

We will now analyze the harmonic approximation in more detail, using the theory of linear viscoelasticity (20). In the case of a homogenous and isotropic material the response to a strain ϵ, that is, the fractional elongation $\Delta L/L_0$, is described by the following equations, which are valid in the static case:

$$\sigma = E \cdot \epsilon \quad \sigma = \eta \cdot \dot{\epsilon} \tag{17}$$

where σ is the stress, the force per area, and E and η are the elastic modulus and the viscosity, respectively. If such a material is exerted to a harmonic strain excitation, the response of the stress is also sinusoidal, but shifted in phase:

$$\epsilon = \epsilon_0 \cdot \sin(\omega t) \quad \sigma = \sigma_0 \cdot \sin(\omega t + \phi). \tag{18}$$

This relation is actually only valid in the steady-state case, when disturbances of the system caused by the onset of the excitation have already decayed. The negligence of this relaxation is valid if the modulation frequencies are small compared to the resonance frequencies of the sample. The complex elastic modulus connects strain and stress in an analogous way to the static case (Eq. 17) and comprises both elastic and viscous parts. This elastic modulus will be in principle a function of the excitation frequency:

$$\sigma_{(\omega)} = E^*_{(\omega)} \cdot \epsilon_{(\omega)}. \tag{19}$$

This complex elastic modulus can be separated either into real and imaginary parts, or into the absolute value and the complex phase angle:

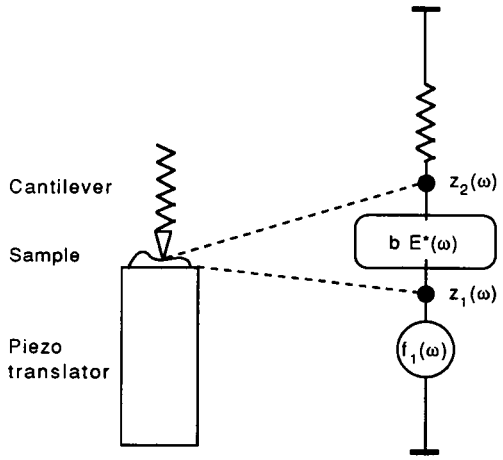

FIGURE 5 Mechanical model and circuit corresponding to the experimental setup for measuring the viscoelastic properties by AFM. The piezo height z_1 is modulated sinusoidally, which will exert the force f_1 to the sample. This force will be transmitted through the sample and leads to a deflection of the cantilever z_2. This modulation of the cantilever will exert another force f_2 to the sample, which will result in an indentation d, depending on its elastic properties $b \cdot E^*$.

$$E^*_{(\omega)} = E'_{(\omega)} + i \cdot E''_{(\omega)} \tag{20a}$$

$$E^*_{(\omega)} = \tilde{E}_{(\omega)} \cdot \exp(i\Theta_{(\omega)}) \tag{20b}$$

where E' and E'' are called storage and loss modulus, respectively, and $\tilde{E}$ and Θ are called the absolute modulus and the loss tangent. The storage modulus, which is proportional to the elastic response, is related to the energy stored during one cycle of excitation. The loss modulus, which is proportional to the viscous response, is related to the energy dissipation during one cycle of excitation (reference 20, p. 55).

In our experimental setup we do not measure strain and stress of the sample directly. We exert a vertical modulation in height to the sample. This modulation is transmitted through the sample to the cantilever, which will be bent to a given extent and thus exert the stress to the sample. The mechanical model and the connected mechanical circuit are depicted in Fig. 5 (reference 20, p. 604). The viscoelastic transfer function of the sample is written as $b \cdot E^*$, where b is the so-called apparatus coefficient, which for the given geometry relates the measurable values force and displacement to the physical values stress and strain. The reciprocal of the apparatus coefficient b will be called the shape factor H.

$$\frac{\epsilon}{\sigma} = b \cdot \frac{z}{F} \quad H = \frac{1}{b}. \tag{21}$$

The sample excitation z_1 is sinusoidal and leads to a phase-shifted response of the cantilever z_2, which is related through the elastic constant E_c, which is the reciprocal of the force constant k_c, of the cantilever to a force F_2 exerted to the sample:

$$z_1 = z_0 \cdot \sin(\omega t) \tag{22a}$$

$$z_2 = z_0' \cdot \sin(\omega t + \phi) \tag{22b}$$

$$F_2 = f_0 \cdot \sin(\omega t + \phi) \tag{22c}$$

$$f_0 = z_0'/E_c. \tag{22d}$$

The mechanical model leads to the following node equations. The algorithm to get these equations is equivalent to Kirchhoff's rules of electrical circuit analysis:

$$F_1(\omega) = b \cdot E^*(\omega) z_1(\omega) - b \cdot E^*(\omega) z_2(\omega) \tag{23a}$$

$$0 = -b \cdot E^*(\omega) z_1(\omega) + (b \cdot E^*(\omega) + E_c) z_2(\omega). \tag{23b}$$

After rearrangement of Eq. 23b and interchange of z_2 by F_2/E_c follows:

$$E^*(\omega) = \frac{HE_c F_2(\omega)}{E_c z_1(\omega) - F_2(\omega)}. \tag{24}$$

Separating this relation into real and imaginary parts, by using formula 22c and the replacement $\gamma = z_0'/z_0$ for the ratio of response and excitation leads to:

$$E'(\omega) = \frac{H\gamma E_c(\cos\phi - \gamma)}{\gamma^2 - 2\gamma\cos\phi + 1} \tag{25a}$$

$$E''(\omega) = \frac{H\gamma E_c \sin\phi}{\gamma^2 - 2\gamma\cos\phi + 1}. \tag{25b}$$

These equations demonstrate that in the general case the elastic properties of the sample are a complicated function of the measurable values, the compression γ and the phase shift ϕ. In the case of the samples discussed below, the phase shift will be very small, because the samples are more elastic than viscous, and the compression γ will be in the order of 1, because the modulation amplitude was kept small. So we can approximate the term $\cos\phi$ as 1. This leads to:

$$E'(\omega) = \frac{\gamma}{1-\gamma} HE_c \tag{26a}$$

$$E''(\omega) = \frac{\gamma}{(1-\gamma)^2} HE_c \sin\phi. \tag{26b}$$

Therefore the amplitude reading of the lockin-analyzer will be proportional to the elastic properties of the sample, and the phase reading will be proportional to the phase shift by the sample, which is a consequence of the viscous properties.

RESULTS AND DISCUSSION

Fig. 6 shows the AFM image of a polymeric DPDA-monolayer on a silicon wafer. The film had been prepared at the air–water interface and was transferred onto the wafer following standard procedures (see reference 12 for details). The film, which on the large scale appeared homogeneous, showed occasionally feather-like distorted areas where the film was torn into individual ribbons. These distortions were created most likely during the transfer from the air–water interface onto the substrate. The measured step height was scan direction dependent, indicating a significant difference in the friction on top of the film and on the bare substrate. After correction of this height anomaly (3, 21) the step height was 25 ± 5 Å, corresponding to the thickness of a monomolecular film. Fig. 6 *b* and 6 *c* show the amplitude and phase images, respectively, which were recorded in parallel to the height image. In the amplitude image, the polymeric film appears darker than the substrate, which means that in these areas the cantilever follows the modulation less well because the film is softer than the substrate. In Fig. 7 a film from the same polymeric amphiphile, but with inclusions of monomeric DMPC, is shown. The step height between the polymeric film and the inclusions which did not significantly differ between back and forth scanning was determined to be 7 ± 1 Å. In the elasicity image (Fig. 7 *b*) the polymeric film appears brighter than the monomeric DMPC inclusions, which means that the DMPC inclusions are softer. Taking into account that the DMPC domains were in the fluid phase when the film was transferred, this result agrees well with our model. Although the modulation response was in these experiments determined quantitatively, the calculation of the elastic moduli from the data is at present extremely inaccurate. Due to the mechanical resonances of the microscope, the excitation amplitude of the sample cannot directly be correlated to the excitation voltage at the piezo. This, together with the largely unknown tip geometry, allows only a qualitative analysis of the effective stiffness of these LB-films.

The phase images (Figs. 6 *c* and 7 *c*) exhibit essentially the same congruent, but inverted, pattern compared to the corresponding elasticity images. In Fig. 6 *c* the phase shift on the polymeric film is lower compared to the background. This means that the polymeric film is more viscous than the substrate. In Fig. 7 *c*, the polymeric film appears darker than the monomeric inclusions. This means that the polymeric film is less viscous then the monomeric inclusions. This finding is qualitatively understandable, taking into account that the DMPC lipids in the amorphous (formerly fluid) phase are less well ordered than in the polymeric film. Unfortunately, we have at present no good model for the dynamics of the tip-sample interaction which would allow a quantitative analysis of the phase shift. However, we can clearly draw the following minimum conclusion from our data: more energy is dissipated in the amorphous regions than in the well ordered polymeric areas. A brief analysis of the hydrodynamic flow of the ambient, which, due to an adsorbed water film might be as viscous as water, shows

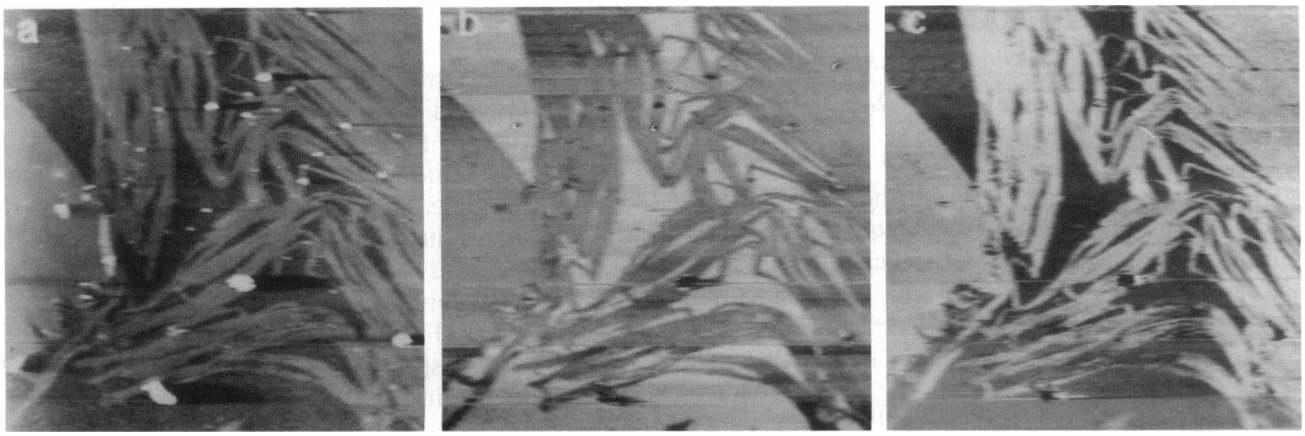

FIGURE 6 AFM images of a polymeric DPDA-monolayer transferred onto a solid support. Fig. *a* shows the height image. Fig. *b* and *c* show the amplitude and phase readings of the lock-in amplifier, which are correlated to the elastic and viscous properties of the sample. Imaging parameters: raw data; constant height mode; size: 7.8 μm; scan speed: 0.6 lines per second; modulation frequency: 15.6 kHz, modulation amplitude: 6 nm; force constant of the cantilever: 64 mN/m.

that at the given frequencies and amplitudes the ambient does not give a significant contribution (3, 22). We also know from high resolution AFM imaging experiments on comparable systems, that under the given experimental conditions the molecular order in the crystalline films is not destroyed (3). We have no direct information, however, on the molecular properties of the lipids in the amorphous areas. We do not know whether or not these lipids are immobile or whether they are laterally displaced by the tip during the modulation. A promising start for a quantitative assessment of the viscosity of crystalline and amorphous lipids might be the work of Evans et al. (23).

So far, we have exploited only the linear response of the sample. The theoretical treatment of the Hertz model had indicated that anharmonic contributions should be negligible. Figure 8 demonstrates that this is true for small modulation amplitudes. It shows a patchy Cd-arachidate film on a silicon wafer. It was partially desorbed by UV irradiation (13) resulting in patches of fatty acid on the bare substrate. The first row of images was recorded at moderate modulation amplitudes of 30 nm. Fig. 8 *a* shows the surface relief, *b* and *c* show the harmonic amplitude and the phase, respectively. Fig. 8 *d* and *e* show the second harmonic amplitude and the second harmonic phase respectively. At these modulation amplitudes the harmonic signals are well detectable whereas the anharmonic response is below the noise level. However, at higher modulation amplitudes, the fatty acid patches give rise to a significant second harmonic signal. As expected, the softer fatty acid paces appear dark in the harmonic amplitude and they also give rise to a higher anharmonic amplitude than the hard substrate. Although the phase angle is higher in the softer

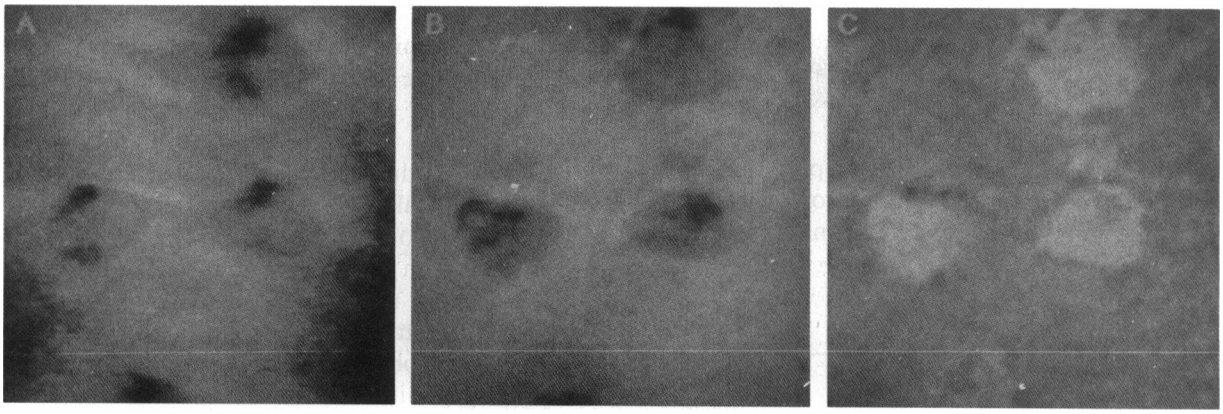

FIGURE 7 AFM images of a polymeric DPDA film containing 30% DPPC. Fig. *a* shows the height image. Fig. *b* and *c* show the amplitude and phase readings of the lock-in amplifier. Imaging parameters: raw data; constant height mode; size: 0.51 μm; scan speed: 0.5 lines per second; modulation frequency: 12.5 kHz, modulation amplitude: 6 nm; force constant of the cantilever: 64 mN/m.

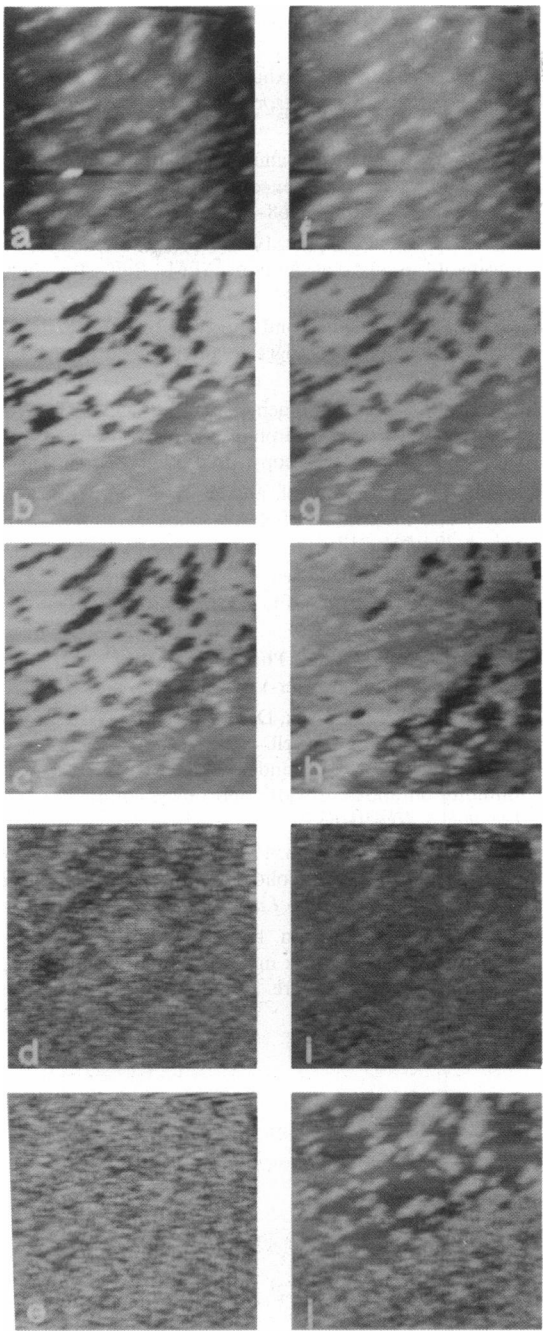

FIGURE 8 AFM images of a Cd-arachidate trilayer on a solid support. The trilayer was partially ablated by UV-irradiation. Fig. *a–e* are recorded while applying moderate modulation amplitudes (30 nm), Fig. *f–j* were recorded at high modulation amplitude (100 nm). The images in the first row are height data, the second and third row are the harmonic amplitude and phase images, respectively, and the fourth and fifth row are the anharmonic amplitude and phase images, respectively. Imaging parameters: size: 15 μm; scan speed: 0.4 lines per second; modulation frequency: 11 kHz, force constant of the cantilever: 64 mN/m.

and more viscous fatty acid domains, these domains appear darker then the substrate. This might be because the phase angle in these experiments crosses zero. In a separate experiment we verified that the nonlinearity of the instrument itself is negligible at these amplitudes, which clearly indicates that certain properties of the sample are responsible for the contrast. One mechanism which we cannot exclude at present is, that in a similar way in which lateral forces contribute to the pseudo height in AFM images via a torsion of the cantilever, this second harmonic signal may be caused by lateral forces. An experiment with direct force modulation or with a four-quadrant photo diode should help to answer this question. The explanation which in our opinion is more likely, however, is that at high amplitudes the Hertz model is not applicable to lipid films any more. It is quite obvious, that when the modulation amplitude becomes comparable to the film thickness, the anisotropy of the elastic properties of the film becomes relevant. One would expect, then, the indentation plot in Fig. 4 to take off at higher amplitudes, giving rise to a considerable anharmonic component. If this interpretation is right, it would quite generally mean that force dependent measurements of the second harmonic response would allow the depth profiling of the viscoelasticity of samples. This might be especially helpful for the investigation of soft layered systems, as they are very common in life sciences.

CONCLUDING REMARKS

A broad spectrum of new measurements is possible by exploiting and manipulating the interaction between tip and sample in a quantitative way. This approach has so far proven to be especially fruitful for soft materials. The strength of AFM-related techniques is that local properties may be accessed at a lateral resolution of molecular dimension. New instrumental designs (C. Prater, personal communication), which employ a direct force modulation by external fields, should help to achieve a comparable resolution also for force modulation microscopy. A richness of new information is then to be expected from force modulation microscopy at mesoscopic magnifications in the cross-over between molecular properties and material properties.

This work was inspired by Harden McConnell and supported by the Deutsche Forschungsgemeinschaft. Fruitful discussions with Hans Ribi are acknowledged.

Received for publication 2 September 1992 and in final form 5 November 1992.

REFERENCES

1. Binnig, G., C. F. Quate, and C. Gerber. 1986. Atomic force microscope. *Phys. Rev. Lett.* 56:930.

2. Drake, B., C. B. Prater, A. L. Weisenhorn, S. A. C. Gould, T. R. Albrecht, C. F. Quate, D. S. Channell, H. G. Hansma, and P. K. Hansma. 1989. Imaging crystals, polymers and biological processes in water with AFM. *Science (Wash. DC).* 243:1586–1589.
3. Radmacher, M., R. W. Tillmann, M. Fritz, and H. E. Gaub. 1992. From molecules to cells—imaging soft samples with the AFM. *Science (Wash. DC).* 257:1900–1905.
4. Weisenhorn, A. L., B. Drake, C. B. Prater, S. A. C. Gould, P. K. Hansma, F. Ohnesorge, M. Egger, S. P. Heyn, and H. E. Gaub. 1990. Immobilized proteins in buffer imaged at molecular resolution by atomic force microscopy. *Biophys. J.,* 58:1251–1258.
5. Heckl, W. 1992. Scanning tunneling microscopy and atomic force microscopy on organic and biomolecules. *Thin solid films,* 210-211:640–647.
6. Engel, A. 1991. Biological applications of scanning probe microscopes. *Annu. Rev. Biophys. Biophys. Chem.,* 20:79–108.
7. Maivald, P., H. J. Butt, S. A. C. Gould, C. B. Prater, B. Drake, J. A. Gurley, V. B. Elings, and P. K. Hansma. 1991. Using force modulation to image surface elasticities with the AFM. *Nanotechnology.* 2:103–106.
8. Pethica, J. B., and W. C. Oliver. 1987. Tip surface interactions in STM and AFM. *Phys. Scr. T19.* 61:61–66.
9. Burnham, N. A., and R. J. Colton. 1989. Measuring the nanomechanical properties and surface forces of materials using an atomic force microscope. *J. Vac. Sci. Technol. A.* 7:2906–2913.
10. Weisenhorn, A. L., M. Khorsandi, S. Kasas, V. Gotozos, M. R. Celio, and H. J. Butt. 1993. Deformation and height anomaly of soft surfaces studied with the AFM. *Nanotechnology.:* In press.
11. Heyn, S. P., R. W. Tillmann, M. Egger, and H. E. Gaub. 1990. A miniaturized micro-fluorescence film balance for protein-containing lipid monolayers spread from a vesicle suspension. *J. Biochem. Biophys. Meth.* 22:145–158.
12. Tillmann, R. W., M. Radmacher, H. E. Gaub, P. Kenny, and H. O. Ribi. 1993. Monomeric and polymeric molecular films from diamino-diethylene glycol-pentacosadiynoic acid. *J. Phys. Chem.* In press.
13. Tippmann-Krayer, P., L. Laxhuber, and H. Möhwald. 1988. Thermal stability and photo desorption of LB films. *Thin solid films,* 159:387–394.
14. Radmacher, M., K. Eberle, and H. E. Gaub. 1992. An AFM with integrated micro fluorescence optics—design and performance. *Ultramicroscopy.* 42-44:968–972.
15. Amer, N. M., and G. Meyer. 1988. A simple method for a remote sensing of stylus deflection in AFM. *Bull. Am. Phys. Soc.* 33:319.
16. Fritz, M., M. Radmacher, and H. E. Gaub. 1992. *In vitro* activation of human platelets triggered and probed by SFM. *Exp. Cell Res.* In press.
17. Tillmann, R. W., M. Radmacher, and H. E. Gaub. 1992. Surface structure of hydrated amorphous silicon oxide at 3 Å resolution by scanning force microscopy. *Appl. Phys. Lett.* 60:3111–3113.
18. Johnson, K. L., K. Kendall, and A. D. Roberts. 1971. Surface energy and the contact of elastic solids. *Proc. R. Soc. London Ser. A.* 324:301–313.
19. Zanoni, R., C. Naselli, J. Bell, G. I. Stegeman, and C. T. Seaton. 1986. Elastic properties of L–B films. *Phys. Rev. Lett.* 57:2838–2840.
20. Tschoegl, N. W. 1989. The Phenomenological Theorie of Viscoelastic Behaviour. Springer-Verlag, Berlin.
21. Thundat, T., R. J. Warmack, D. P. Allison, L. A. Bottomley, A. J. Lourenco, and T. L. Ferrell. 1992. Atomic force microscopy of deoxyribonucleic acid strands adsorbed on mica: The effect of humidity on apparent width and image contrast. *J. Vac. Sci. Technol. A.* 10:630–635.
22. Rädler, J., and E. Sackmann. 1992. On the measurement of weak repulsive and frictional colloidal forces by reflection interference contrast microscopy. *Langmuir.* 8:848–853.
23. Evans, E., and E. Sackmann. 1988. Translational and rotational drag coefficients for a disk moving in a liquid membrane associated with a rigid structure. *J. Fluid Mech.* 194:553–561.